Aquatic Toxicology 267 (2024) 106839

Contents lists available at ScienceDirect

Aquatic Toxicology

journal homepage: www.elsevier.com/locate/aqtox

Perfluorooctane sulfonate causes pyroptosis and lipid metabolism disorders through ROS-mediated NLRP3 inflammasome activation in grass carp hepatocyte

Bendong Shi [a], Zhuoqi Zhang [a], Jiao Xing [c], Qiaohan Liu [a], Jingzeng Cai [a], Ziwei Zhang [a,b,*]

[a] College of Veterinary Medicine, Northeast Agricultural University, Harbin 150030, PR China
[b] Key Laboratory of the Provincial Education Department of Heilongjiang for Common Animal Disease Prevention and Treatment, College of Veterinary Medicine, Northeast Agricultural University, Harbin 150030, PR China
[c] China Institute of Water Resources and Hydropower Research, Beijing 100038, China

ARTICLE INFO

Keywords:
Perfluorooctane sulfonate
Grass carp hepatocyte
Pyroptosis
Lipid metabolism
Inflammatory cytokines

ABSTRACT

The surfactant perfluorooctane sulfonate (PFOS) is widely produced worldwide. It is a persistent organic pollutant in the aquatic environment and poses a serious threat to aquatic organisms, as PFOS exposure can cause liver injury in a wide range of organisms. However, it is unclear whether PFOS exposure-induced hepatocellular injury in fish is associated with ROS-mediated activation of NLRP3 inflammasome. In this study, various PFOS concentrations were applied to L8824 cells, a cell line of grass carp hepatocytes. The detrimental impacts of PFOS on oxidative stress, pyroptosis, lipid metabolism, and the discharge of inflammatory factors were examined. MCC950 and N-acetylcysteine were employed to hinder the PFOS-stimulated activation of the NLRP3 inflammasome and the excessive generation of reactive oxygen species in L8824 cells, respectively. This study demonstrated that treatment with PFOS resulted in oxidative stress and activation of NLRP3 inflammasome in L8824 cells. This led to increased expression levels of indicators related to pyroptosis, accompanied by the upregulation of pro-inflammatory cytokine expression as well as downregulation of anti-inflammatory factors. In addition, following PFOS exposure, the expression levels of genes related to lipid synthesis were upregulated and lipid catabolism-related genes were downregulated. Surprisingly, both N-acetylcysteine and MCC950 interventions significantly reduced PFOS-induced L8824 cell pyroptosis and lipid metabolism disorders. In conclusion, this research demonstrated that PFOS drives NLRP3 inflammasome activation through oxidative stress induced by reactive oxygen species overload. This in turn leads to pyroptosis and lipid metabolism disorders.

1. Introduction

Perfluoroalkyl and polyfluoroalkyl substances (PFAS) are extensively utilized in daily consumer goods and industrial products because of their exceptional water resistance and surfactant properties (Buck et al., 2011). Perfluorooctane sulfonate (PFOS) - a specific type of PFAS - has the highest detection rate and concentration levels in both the environment and body tissues. The main sources of PFOS in the environment are industrial and domestic wastewater discharge and the use of fire-fighting agents (Luo et al., 2023; Foord et al., 2024). The pesticide sulfluramid can be metabolized to PFOS in the environment, and its extensive use is also an important factor contributing to the considerably elevated levels of PFOS in the environment (Barbosa Machado Torres et al., 2022; Guida et al., 2023). Because of its extensive production, excessive usage, and improper disposal practices, PFOS has been widely detected in various environmental matrices, including air, surface water, house dust, sediment, and soil. (Wong et al., 2018; Harrad et al., 2019; Chu et al., 2022; Liu et al., 2022b; Wang et al., 2023d). PFOS can persist in the environment and enter the body through occupational exposure as well as through physical contact with products containing PFOS, where it accumulates in the blood, liver, kidneys, and breast milk (Wang et al., 2022). Research confirmed that PFOS exposure can damage several organs because of its neurotoxicity, pulmonary toxicity, reproductive toxicity, nephrotoxicity, immunotoxicity, and hepatotoxicity (Chen et al., 2012; Lee et al., 2021, 2022; Jiang et al., 2022; Liang et al., 2022; Zhang et al., 2022a). It has been reported that the PFOS

* Corresponding authors at: College of Veterinary Medicine, Northeast Agricultural University, Harbin 150030, PR China
E-mail address: zhangziwei@neau.edu.cn (Z. Zhang).

https://doi.org/10.1016/j.aquatox.2024.106839
Received 26 November 2023; Received in revised form 6 January 2024; Accepted 12 January 2024
Available online 13 January 2024

Table 1
mRNAs primer seque.

Genes	Primer Sequence (5′–3′)
NLRP3	Forward: AGGCTACAGGTGTCTCAGTGGAAC
	Reverse: GCAGCAGCCTCAGAAGACATTCC
Caspase-1	Forward: CTCGCTGCTCTTGTTGCTAGAAGG
	Reverse: TTCAAGTTGGCCGTGCAGATAGTG
IL-18	Forward: AAGAGCGGAATAAGGAGCAATGC
	Reverse: TGCTTACAAGGTGATGTCACAGAG
IL-1β	Forward: CTCCGCTCCACATCTCGTACTC
	Reverse: CATCTCCACCATCTGCGAATCTTC
IL-4	Forward: GAGCACCAGAACCGAACAAG
	Reverse: GAGAAATGCAAAGAAGAGGC
IL-10	Forward: TGGAGACCATTCTGCCAACAG
	Reverse: CCATATCCCGCTTGAGTTCCT
TNF-α	Forward: ACCAGGCTTTCACTT
	Reverse: TAGCCGCCATAGGAATCGGA
IFN-γ	Forward: TGTGCCCGAGAACCTAGACA
	Reverse: AGGATTCGCAGGAAGATGGG
IL-6	Forward: CGGTCCACTCGATCCTGTTC
	Reverse: CCTCTTGGGGTCTTTCCCTC
IL-8	Forward: ACCCTCCTAGCCCTCACTGT
	Reverse: CATGGTGCTTTGTTGGCAAGG
HSL	Forward: TGGAACGTTACTGAGTCTGG
	Reverse: AAGCGCACGTTGACTGG
UCP-1	Forward: CGTGGTTTGTGGAAAGG
	Reverse: GCTCCAAATGCAGATGTG
ATGL	Forward: TCGTGCAAGCGTGTATATG
	Reverse: GCTCGTACTGAGGCAAATTA
ACCα	Forward: TGGAGGTGGCCTTCAACAATACCA
	Reverse: AAGGGTCCATGATGACAGTTGGGA
CPT-1	Forward: GTTACACTGGATGACACAGAG
	Reverse: TTAAGGCCCATAGTTCCATTC
PPAR-γ	Forward: GCATCTGTACGAGTCCTATCT
	Reverse: GAGACTTCATGTCGTGGATAAC
SCD-1	Forward: ACTGGAGCTCTGTATGGAC
	Reverse: CGTAGATGTCATTCTGGAAG
LPL	Forward: TAGCGAAGAACCCGAAGAAG
	Reverse: ACCAGTCCACCACAATCACA
FANS	Forward: CCATGCATTTGTTGGTCTTG
	Reverse: TCCTCTCCAGTAAGCGGCTA
DGAT1α	Forward: ACGAGACATCCGCGAGTAAA
	Reverse: TGCATTGGACAGAACCAGCA
ACTB	Forward: GATGGACTCTGGTGATGGTGTGAC
	Reverse: TTTCTCTTTCGGCTGTGGTGGTG

concentration in ordinary surface water ranges from 0.1 to 100 ng/L, but in rivers around fluorochemical production enterprises, PFOS has been detected at concentrations of up to 600 ng/L (Mahapatra et al., 2023). A recent study showed that PFOS promotes IL-1β secretion and pyroptosis by activating the AIM2 inflammasome, thereby leading to pulmonary, renal, and hepatic inflammation and injury (Wang et al., 2021). Another study indicated that PFOS induced ferroptosis in HUVEC cells by modulating the expression level of the proteins GPX4 and ACSL4, ultimately resulting in the dysfunction of endothelial cells (Cui et al., 2022). PFOS exposure can also lead to lysosomal membrane permeability of HepG2 cells, thereby blocking autophagy flux, which results in excessive accumulation of autophagosomes, and transforms autophagy into a destructive process (Yao et al., 2014). Previous research showed that PFOS in water bodies can be bioconcentrated through the food chain (Zareitalabad et al., 2013). A potential risk assessment, based on Environment Quality Standards, has shown substantial contamination of PFOS in fish. Zhu et al. found that PFAS concentration in the fish liver surpassed that in fish muscles, with PFOS being the most predominant PFAS present (Xin et al., 2023).

Oxidative stress is a chemical process that can generate both reactive oxygen species (ROS) and free radicals. Excessive production of ROS and free radicals has been shown to lead to tissue and cellular damage (Yang et al., 2019). Multiple studies have shown that ROS can cause lipid peroxidation, DNA damage, and inflammatory reactions (Liu et al., 2023; Ma et al., 2023; Wang et al., 2023b). The NLRP3 inflammasome has been identified as a crucial mediator in the pathogenesis of various inflammatory diseases (Lo et al., 2023). ROS overproduction stimulated by stressors has been reported to upregulate NF-κB expression, which in turn promotes activation of downstream factors, including the NLRP3 inflammasome, Caspase-1, and the precursors of IL-1β and IL-18 (Gao et al., 2022; Shang et al., 2023). Activated Caspase-1 can effectively cleave the gasdermin D (GSDMD) protein, thus creating the GSDMD-N peptide fragment containing the active domain of GSDMD that initiates cell membrane rupture and pore formation. This process leads to the release of cellular contents and eventually results in cellular pyroptosis. In addition, activation of Caspase-1 stimulates the maturation and release of IL-18 and IL-1β, both of which enhance the aggregation of inflammatory cells and escalate the inflammatory response (Cai et al., 2021; Liu et al., 2022a; Zhang et al., 2022b). Recent research has demonstrated that polystyrene nanoparticles potentially initiate hepatic inflammation via the ROS-NLRP3 signaling pathway (Chi et al., 2022). Shi et al. (2023) demonstrated that bisphenol A can cause cellular pyroptosis by increasing oxidative stress, therefore exacerbating hepatic inflammation. Yang et al. (2022) demonstrated that the T-2 toxin activates regulation of the NLRP3 inflammasome by promoting ROS production, leading to inflammatory damage in both testicular tissue and TM4 cells. NLRP3 is widely regarded as a potent signaling molecule that governs a range of cellular responses, including lipid metabolism and inflammatory reactions (Tilg et al., 2021). Wang et al. (2023c) demonstrated that perfluorodecanoic acid promotes adipogenesis in 3T3-L1 and HepG2 cells through a pathway mediated by the NLRP3 inflammasome. Zhao et al. (2021) showed that fructose regulates the lipid metabolism by activating NLRP3 inflammasome regulation and increasing the production of inflammatory cytokines, leading to lipid deposition in the liver. Wu et al. (2021) found that diabetes-induced glomerular lipid accumulation could be reversed in NLRP3 knockout

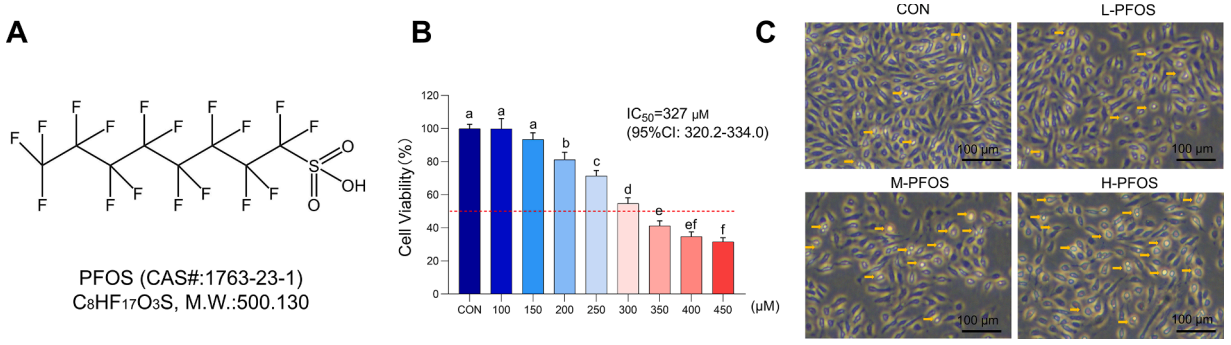

Fig. 1. Cell viability determination and morphological observation. (A) Molecular structure of PFOS. (B) Changes in cell viability following treatment with various concentrations of PFOS. (C) L8824 cell changes after exposure to 0 μM, 150 μM, 200 μM, and 250 μM PFOS were observed under a microscope. Scale bars: 100 μm. The means ± SEM ($n = 3$) was used to present the experimental data. Significant differences among groups were denoted by variations in letters ($P < 0.05$). Conversely, groups with the same letters were considered not to have significant differences ($P \geq 0.05$).

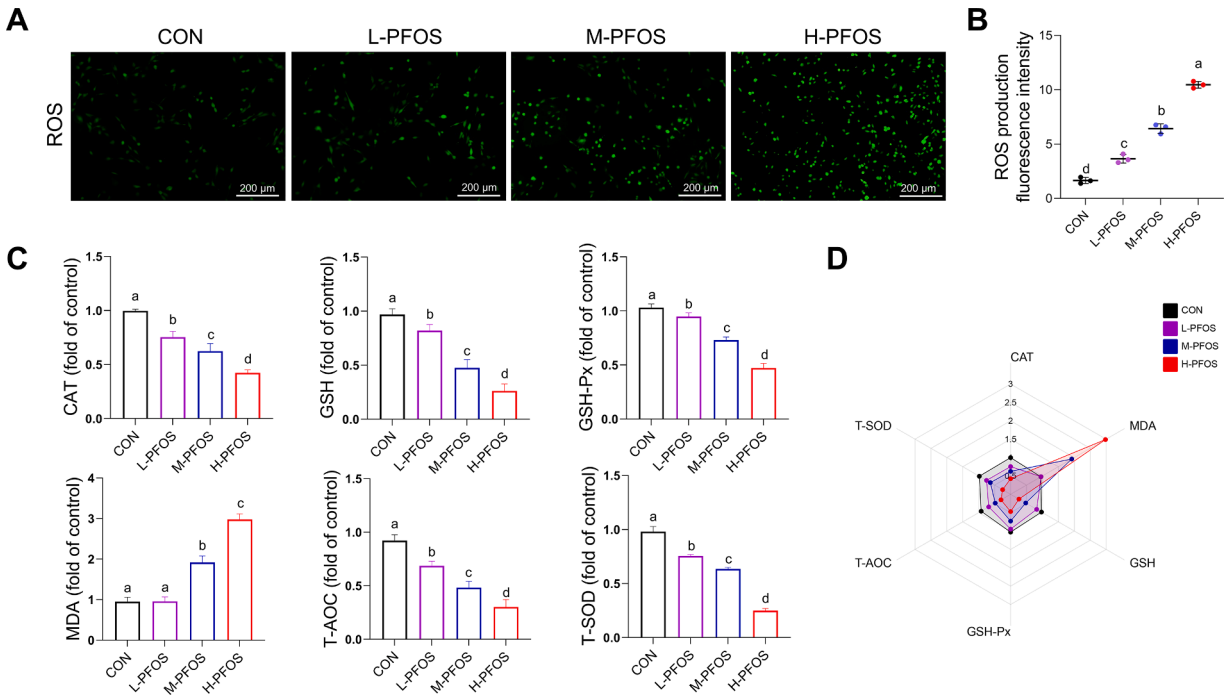

Fig. 2. Effect of PFOS on oxidative stress of L8824 cells. (A-B) DCFH-DA fluorescent probe staining and quantitative analysis of L8824 cells. (C) GSH, CAT, GSH-Px, T-AOC, and T-SOD activities, as well as MDA content, were measured in L8824 cells following treatment with varying concentrations of PFOS. (D) Radar charts displaying alterations in measures of oxidative stress. The means ± SEM ($n = 3$) was used to present the experimental data. Significant differences among groups were denoted by variations in letters ($P < 0.05$). Conversely, groups with the same letters were considered not to have significant differences ($P \geq 0.05$).

mice; *in vitro* assays demonstrated that MCC950 or NLRP3 siRNA treatment significantly alleviated glucose-induced lipid accumulation in podocytes. Hu et al. (2015) demonstrated that increased ROS accumulation in the heart can activate the regulatory NLRP3 inflammasome, which in turn disturbs the lipid metabolism in dogs with myocardial ischaemia via PPAR-α overexpression.

Numerous tests have demonstrated that PFOS exposure can damage terrestrial and aquatic organisms (Mao et al., 2023; Wang et al., 2023a). The grass carp has emerged as an economically important freshwater fish in China owing to its well-established aquaculture techniques, cost-effective approach, minimal management challenges, satisfactory breeding prospects, and sustained consumer demand. As the largest detoxification organ, the liver has the capacity to either metabolize toxic substances into intermediate metabolites or neutralize them completely, producing water-soluble substances that can be excreted in urine. Studies have found that PFOS exposure can result in different types of cell damage. However, the mechanism underlying the toxicological damage caused by exposure to various doses of PFOS in grass carp hepatocytes remains unknown. In this study, L8824 cells were used to establish an *in vitro* PFOS exposure model. The presence of oxidative stress was confirmed through the detection of pro-oxidation indicators (ROS and MDA) and the activities of antioxidant enzyme (CAT, GSH, GSH-Px, T-AOC, and T-SOD). Immunofluorescence double staining was used to detect the expression levels of NLRP3 and GSDMD. Western blot and qRT-PCR were utilized to determine the expression levels of genes related to pyroptosis, inflammatory cytokines, and lipid metabolism. Intracellular lipid deposition was detected by Oil-red O staining. This study demonstrates how PFOS interferes with pyroptosis and lipid metabolism disorders in L8824 cells. This research provides a theoretical foundation for PFOS toxicology research and a novel perspective on safeguarding aquatic creatures.

2. Materials and methods

2.1. Cell culture

Grass carp hepatocytes (L8824 cells) were obtained from the China center for type culture collection. L8824 cells were removed from liquid nitrogen and rapidly rewarmed by slow shaking in a water bath at 28.5 °C. Cells were then transferred to a 4-fold volume of medium (Medium 199/EBSS, biosharp, the composition of which is stated below) and then centrifuged at 1000 rpm for 8 min. Subsequently, the top liquid layer of the centrifuge tube was discarded, and the cells were re-suspended by adding M199 complete medium. M199 complete medium is composed of M199 basal medium plus a mixture of 10 % FBS (Opcel Biotechnology Co., Ltd., Inner Mongolia, China) and 1 % penicillin-streptomycin solution (Procell Life Science & Technology Co., Ltd., Wuhan, China). The resuspended cells were transferred to a cell culture flask and shaken slowly to ensure even distribution of the resuspended cells throughout the culture flask. L8824 cells were cultured at a temperature of 28.5 °C and in an atmosphere containing 5 % CO_2 for a duration of 48 h, after which they were passaged (Cai et al., 2023b; Li et al., 2023b).

2.2. Cell viability assay

Perfluorooctane sulfonate was purchased from the Laboratory of the Government Chemist (Teddington, UK), dissolved in DMSO (Biotopped, Beijing, China), and a stock solution was prepared. To eliminate any potential influence of DMSO on cellular injury, the DMSO concentration in the medium was consistently maintained below 0.05 % during the entirety of the experimental study. Hepatocytes were uniformly distributed in 96-well plates at a density of 1×10^6 cells/mL and then cultured by adhesion to the wall at 28.5 °C for 24 h under 5 % CO_2. Subsequently, hepatocytes were exposed to varying final concentrations of PFOS (100, 150, 200, 250, 300, 350, 400, and 450 μM) for 24 h. L8824 cells were carefully rinsed with PBS and subsequently incubated

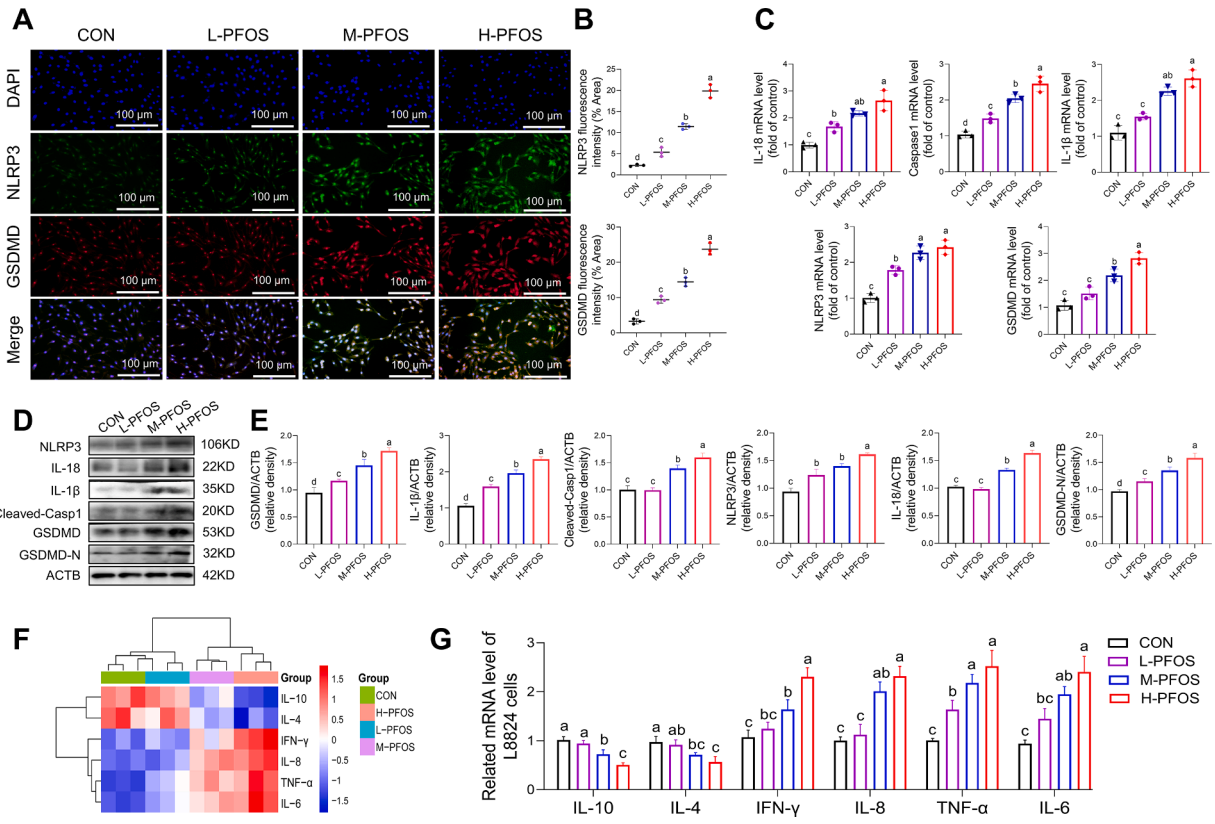

Fig. 3. Effect of PFOS exposure on pyroptosis of L8824 cells. (A, B) Immunofluorescence was employed to identify NLRP3 expression (green) and GSDMD expression (red) in cells from respective treatment groups and to quantify fluorescence intensity. Scale bars: 100 μm. (C) The mRNA abundance of NLRP3, Caspase-1, GSDMD, IL-1β, and IL-18. (D, E) Expression results and quantitative analysis of NLRP3, GSDMD, GSDMD-N, Cleaved-Casp-1, IL-1β, and IL-18 at the protein level. Heatmap (F) and quantitative bar graph (G) of mRNA expression levels related to inflammatory cytokines (i.e., IL-10, IL-4, IFN-γ, IL-8, TNF-α, and IL-6) in L8824 cells exposed to PFOS. The means ± SEM ($n = 3$) was used to present the experimental data. Significant differences among groups were denoted by variations in letters ($P < 0.05$). Conversely, groups with the same letters were considered not to have significant differences ($P \geq 0.05$).

with 100 μL of M199 medium containing the CCK-8 working solution (Saint-Bio, Shanghai). Finally, the absorbance of each well was measured using a microplate reader.

2.3. Cell treatment

Cells were spread evenly in 6-well plates and cultured for 24 h. Cells were then treated with various final concentrations of PFOS for 24 h. Considering that the corresponding survival rate at 300 μM PFOS exposure was only 54.72 %, 0 μM (CON), 150 μM (L-PFOS), 200 μM (M-PFOS), and 250 μM (H-PFOS) were chosen as experimental exposure concentrations. In mechanism validation experiments, hepatocytes were initially pretreated with either the ROS scavenger N-acetylcysteine (NAC) (5 mM for 1 h) or the NLRP3 inhibitor MCC950 (10 μM for 30 min), followed by PFOS exposure at a final concentration of 200 μM for a duration of 24 h. Subsequently, hepatocytes were collected for analysis. NAC and MCC950 were purchased from Medchemexpress (Monmouth Junction, NJ, USA).

2.4. Oxidative stress analysis

DCFH-DA was diluted with a serum-free medium at a 1:1000 ratio to a final concentration of 10 μmol/L. DCFH-DA dilutions were added to the cells of different treatment groups, which were then incubated under suitable conditions for 40 min (Li et al., 2023a). Fluorescence images were captured using a fluorescence microscope (Olympus, IX53, Japan), and subsequently quantified utilizing Image J software (National Institutes of Health, Bethesda, USA). The treated cells were lysed and centrifuged, and the supernatants were collected. MDA, GSH-Px, GSH, CAT, T-AOC, and T-SOD levels in cells were measured using commercial kits based on the instructions provided by the manufacturers.

2.5. Oil red O staining

After the cell treatment at different conditions, 4 % paraformaldehyde fixative was added and cells were fixed for 20 min. PBS (1 mL) was added to each well, cells were covered for 20 s and then PBS was removed; the appropriate amount of Oil red O staining working solution was added (Beyotime, China) and the mixture was stained for 20 min. Then, the cells were observed and photographed under an optical microscope (Nikon 80i, Nikon Corporation, Japan). Finally, intracellular lipid deposition was quantitatively analyzed using Image J software (National Institutes of Health, Bethesda, USA).

2.6. Immunofluorescence

Cells from different treatment groups were subjected to fixation using a 4 % paraformaldehyde solution, followed by encapsulation in a containment solution containing 5 % BSA. Then, cells were incubated with an anti-NLRP3 primary antibody at a temperature of 4 °C overnight, followed by washing with TBST. Subsequently, the cells were incubated with a Dylight 488 goat anti-rabbit IgG (1:1000, Biodragon, China) for 1.5 h at 37 °C, while being protected from light. Then, cells were incubated with anti-GSDMD primary antibody for 2 h at 37 °C (protected from light) and then incubated with Dylight 594 goat anti-mouse IgG (1:1000, Biodragon, China) for 1 h at 37 °C (also protected from light). Nuclei were counterstained with DAPI (Beyotime, China) at room temperature for a period of 15 min (Shi et al., 2023). Finally, the

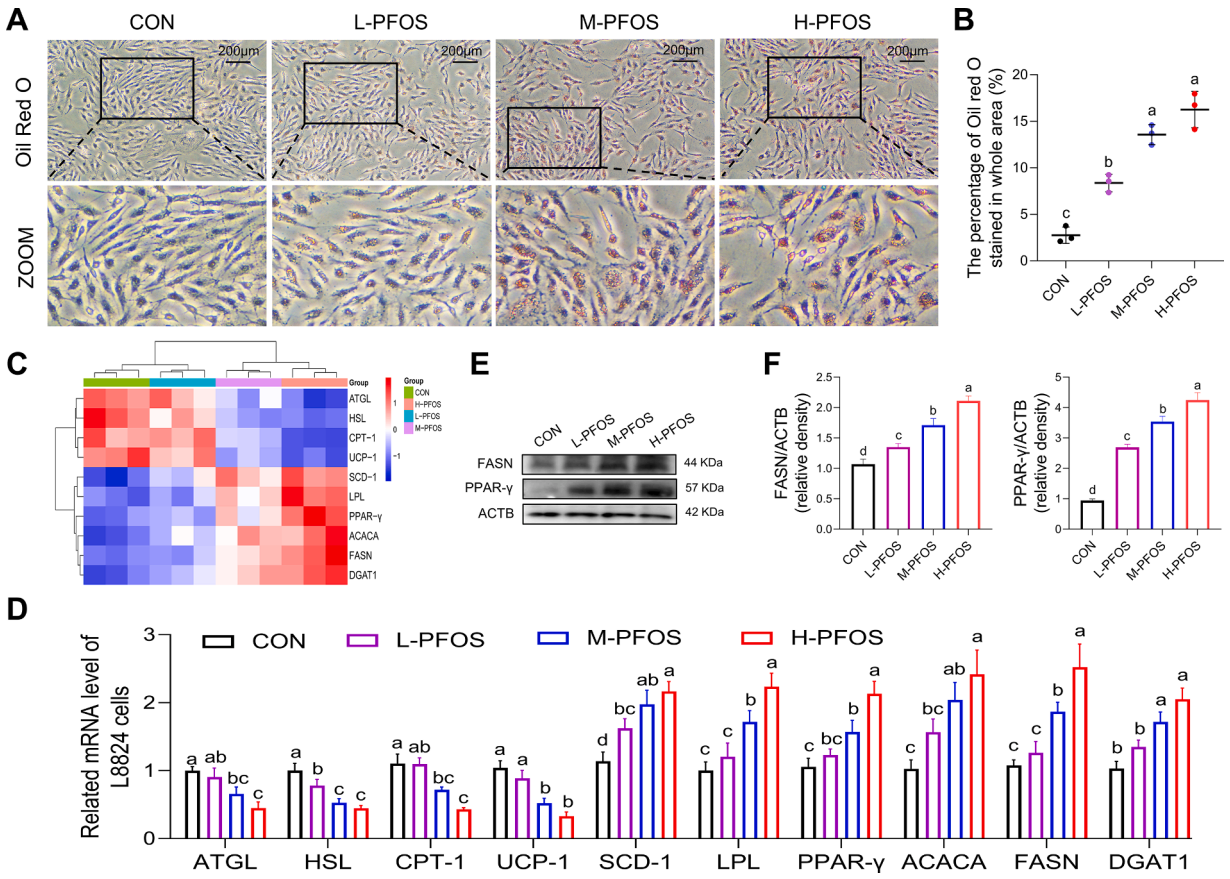

Fig. 4. The effect of PFOS on the lipid metabolism of L8824 cells. (A, B) Observation of PFOS-induced Lipid deposition in L8824 cells and quantitative analysis of positive area. Scale bars: 200 μm. Heatmap (C) and quantitative bar graph (D) of mRNA expression levels related to lipid synthesis (i.e., LPL, FASN, PPAR-γ, ACCα, DGAT1α, SCD-1) and lipid catabolic (i.e., UCP-1, ATGL, HSL, CPT-1) in L8824 cells under PFOS exposure. (E, F) The results of lipid synthesis-related protein (i.e., PPAR-γ and FASN) expression at protein levels. The means ± SEM ($n = 3$) was used to present the experimental data. Significant differences among groups were denoted by variations in letters ($P < 0.05$). Conversely, groups with the same letters were considered not to have significant differences ($P \geq 0.05$).

fluorescence intensity of images captured by fluorescence microscopy (Olympus, IX53, Japan) was quantitatively analyzed using Image J software (National Institutes of Health, Bethesda, USA).

2.7. Real-time quantitative PCR

RNA extraction was performed using a conventional Trizol reagent as described previously, and the concentration and purity of RNA were determined spectrophotometrically (Yao et al., 2023b). The synthesis and reverse transcription of cDNA were conducted following the protocol provided by the cDNA first strand synthesis kit (TransGen, China). The primer sequences used in this study are listed in Table 1. ACTB was employed as an internal reference gene, and gene expression levels were quantified using the $2^{-\Delta\Delta Ct}$ method (Cai et al., 2023a; Dong et al., 2023).

2.8. Western blotting

Western blotting was conducted in reference to a previous description of the experimental procedure (Yao et al., 2023a). RIPA lysate containing PMSF protease inhibitor was added to differently treated cells for ultrasonic lysis in a cold environment. The protein concentration was measured in the supernatants of every experimental group using a BCA protein quantification kit (Solarbio, China). Protein samples from different treatment groups were added to a pre-prepared SDS-PAGE gel for electrophoretic separation, and the separated proteins were wet transferred to an NC membrane at 200 mA. Skimmed milk powder (5 %) was used to seal the treatment for 2 h, and then, the sealed NC membrane was incubated overnight with the following primary antibodies: ACTB, NLRP3, Cleaved-Casp-1, IL-1β, IL-18 (Wanleibio, China), PPAR-γ, FASN (Immunoway, USA), GSDMD, and GSDMD-N (Abclonal, China). Next, NC membranes with completely bound primary antibodies were incubated with HRP-coupled secondary antibody dilutions for 2 h. Finally, target protein bands were visualized utilizing an ECL kit (Meilunbio, China), and membranes were scanned with an Azure imaging Biosystem C300 (Thermo, USA). The quantitative grey value statistics of the target protein bands were analyzed using ImageJ software (National Institutes of Health, Bethesda, USA).

2.9. Bioinformatics analysis

R packages (pheatmap and corrplot) were utilized to analyze the correlation between cellular pyroptosis, inflammatory cytokines, and lipid metabolism genes. The protein-protein interaction networks for differentially expressed proteins were constructed using the online database STRING 11.5 (https://cn.string-db.org). Furthermore, pathway enrichment analysis of differentially expressed proteins was conducted using Metascape (https://metascape.org).

2.10. Statistical analysis

Data are presented as means ± SEM ($n = 3$). Statistical analysis of the experimental data was carried out using GraphPad Prism (version 9.0). One-way ANOVA was used to analyze differences between groups. The result of the Shapiro-Wilk Normality test showed that these data are normally distributed. Different letters indicate significant differences between groups ($P < 0.05$), while the same letter indicates non-

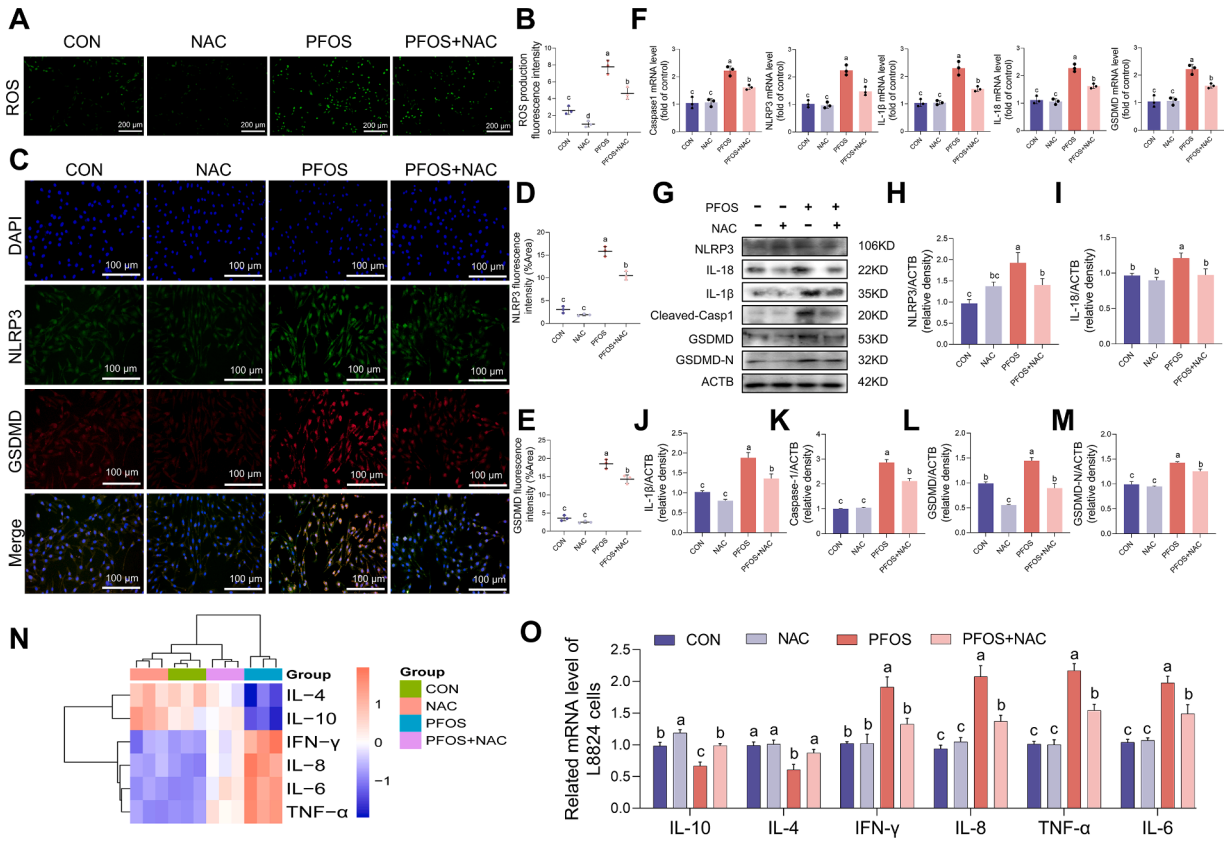

Fig. 5. Effects of NAC on PFOS-induced pyroptosis and inflammatory cytokine release in L8824 cells. (A, B) Detection of ROS levels using DCFH-DA fluorescence labeling and quantitative analysis using Image J software. Scale bars: 400 μm. (C–E) Immunofluorescence was employed to identify NLRP3 expression (green) and GSDMD expression (red) in cells from respective treatment groups and to quantify fluorescence intensity. Scale bars: 100 μm. (F) NLRP3, Caspase-1, GSDMD, IL-1β, and IL-18 mRNA expression abundance of genes. (G–M) NLRP3, GSDMD, GSDMD-N, Cleaved-Case-1, IL-1β, and IL-18 protein bands and quantitatively analyzed. Heatmap (N) and quantitative bar graph (O) of mRNA expression abundance of inflammatory factors (i.e., IL-10, IL-4, IFN-γ, IL-8, TNF-α, IL-6) in L8824 cells treated with PFOS and NAC. The means ± SEM ($n = 3$) was used to present the experimental data. Significant differences among groups were denoted by variations in letters ($P < 0.05$). Conversely, groups with the same letters were considered not to have significant differences ($P \geq 0.05$).

significant differences between groups ($P > 0.05$).

3. Results

3.1. PFOS exposure induced morphological damage and viability reduction in L8824 cells

As shown in Fig. 1B, the survival of L8824 cells decreased progressively in a dose-dependent manner in response to exposure to increasing levels of PFOS. The IC_{50} of L8824 cells after 24 h of exposure to PFOS-containing medium was 327 μM. The effect of PFOS exposure on the morphology of L8824 cells is depicted in Fig. 1C. PFOS exposure elicits alterations in the count of adherent cells, leading to a notable increase in the population of cells featuring a rounded morphology (as indicated by arrows).

3.2. PFOS exposure induced oxidative stress in L8824 cells

Fig. 2A and B indicate that with increasing concentration of PFOS, the intracellular ROS level increased significantly. PFOS exposure significantly elevated the levels of MDA while simultaneously suppressing the activities of GSH, GSH-Px, T-SOD, CAT, and T-AOC compared to the CON group. In particular, the activities of antioxidant enzymes decreased gradually and significantly with increasing PFOS exposure dose (Fig. 2C). Subsequently, the transformed data of oxidative stress indicators were analyzed and depicted as a radar map (Fig. 2D). The six directional axes in the chart represent the six types of oxidative stress indicators. The normalized data for these six oxidative stress indicators under different exposure treatments demonstrated that exposure to PFOS significantly induced MDA. Taken together, exposure to PFOS can cause an overload of ROS and oxidative stress.

3.3. PFOS exposure induced pyroptosis and the release of inflammatory cytokines in L8824 cells

To confirm the occurrence of pyroptosis, the expression abundance of markers related to the NLRP3 inflammasome-mediated pyroptosis pathway was assessed using qRT-PCR, Western blotting, and immunofluorescence. As demonstrated by representative immunofluorescence images shown in Fig. 3A and B, the intensity of fluorescence measurements of NLRP3 (green) and GSDMD (red) in the group treated with PFOS increased progressively with increasing PFOS concentrations. As shown in Fig. 3C, the mRNA expression abundance of NLRP3, Caspase-1, GSDMD, IL-1β, and IL-18 in cells was also significantly increased with increasing PFOS concentration. Similarly, the expression abundances of NLRP3, GSDMD, GSDMD-N, Cleaved-Caspase-1, IL-1β, and IL-18 proteins increased significantly with increasing concentration of PFOS compared to the CON group (Fig. 3D and E). In addition, as shown in Fig. 3F and G, the mRNA expression levels of IL-6, IL-8, IFN-γ, and TNF-α increased significantly with increasing PFOS concentration. In contrast, the mRNA expression abundance of IL-4 and IL-10 decreased significantly with increasing PFOS concentration. Because of these findings, it was hypothesized that PFOS can induce pyroptosis and the release of inflammatory cytokines in L8824 cells.

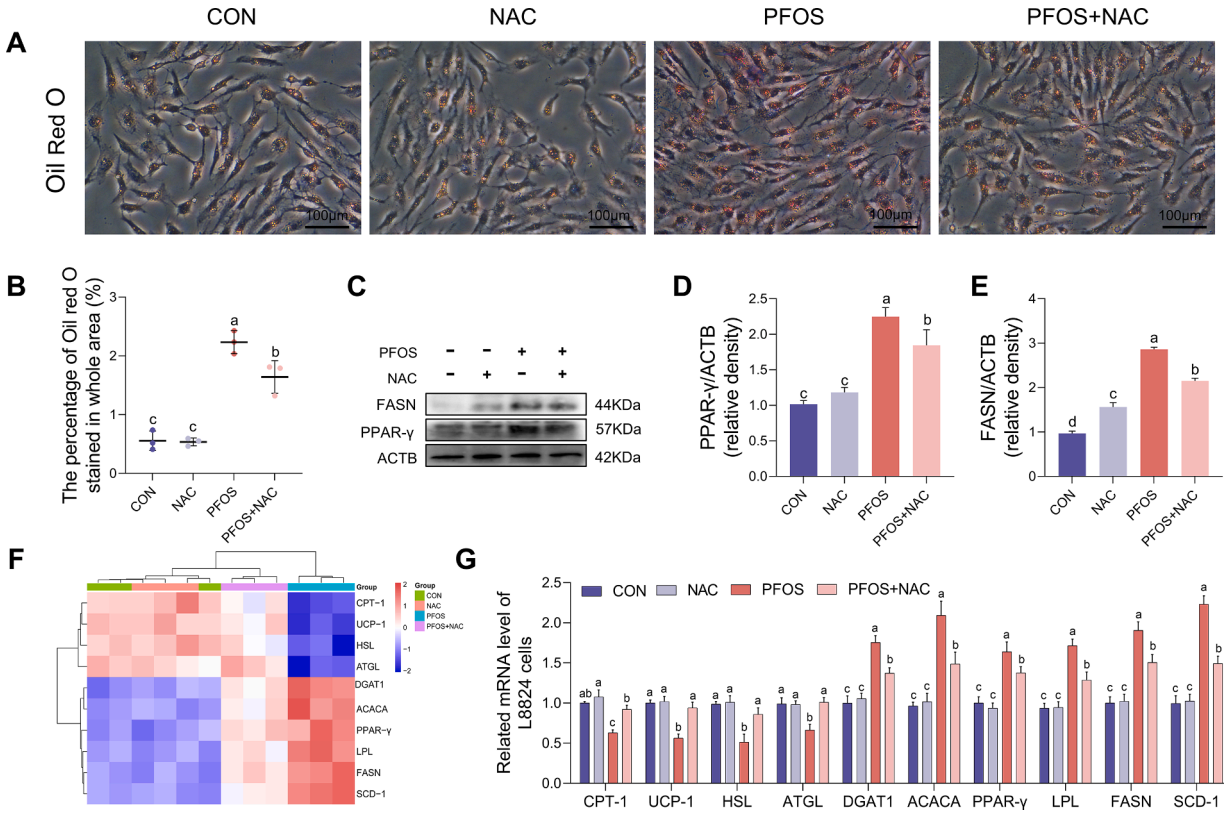

Fig. 6. NAC alleviated the effect of PFOS on lipid metabolism disorder in L8824 cells. (A, B) Oil red O staining and ImageJ quantitative analysis were used to observe the effect of NAC on lipid deposition in L8824 cells exposed to PFOS. Scale bars: 100 μm. (C–E) Results and quantitative analysis of lipid synthesis genes (PPAR-γ and FASN) expression at the protein level. Heatmap (F) and quantitative bar graph (G) of mRNA expression levels related to lipid synthesis (i.e., LPL, FASN, PPAR-γ, ACCα, DGAT1α, SCD-1) and lipid catabolic (i.e., UCP-1, ATGL, HSL, CPT-1) in L8824 cells under PFOS and NAC co-treatment. The means ± SEM ($n = 3$) was used to present the experimental data. Significant differences among groups were denoted by variations in letters ($P < 0.05$). Conversely, groups with the same letters were considered not to have significant differences ($P \geq 0.05$).

3.4. *PFOS exposure induced lipid metabolism disorders in L8824 cells*

Oil Red O staining demonstrated a minimal presence of oil droplets in the CON group, while L8824 cells treated with PFOS showed large areas containing oil droplets (Fig. 4A). Quantification of the area of positively stained regions demonstrated a significant augmentation of lipid build-up in L8824 cells with increasing concentrations of PFOS compared to the CON group (Fig. 4B). Moreover, PFOS can promote the expression level of genes related to lipid synthesis (i.e., LPL, FASN, PPAR-γ, ACCα, DGAT1α, and SCD-1) and reduce the expression level of genes related to lipid catabolism (i.e., UCP-1, ATGL, HSL, and CPT-1), which is positively correlated with the treatment concentration (Fig. 4C and D). As illustrated in Fig. 4E and F, the abundance of proteins associated with lipid synthesis (i.e., PPAR-γ and FASN) showed a significant increase with increasing PFOS concentration compared to the CON group. These results suggest that PFOS can induce lipid deposition in L8824 cells *in vitro*.

3.5. *ROS inhibition alleviated PFOS exposure-induced pyroptosis and inflammatory cytokines release in L8824 cells*

Pre-administration of NAC significantly decreased the level of ROS production caused by PFOS exposure compared to the PFOS alone treatment group (Fig. 5A and B). The results of immunofluorescence imaging showed a significant decrease in the fluorescence intensity of NLRP3 (green) and GSDMD (red) proteins in the PFOS+NAC co-treatment group compared to the PFOS treatment group alone (Fig. 5C–E). The mRNA expression abundance of NLRP3, IL-1β, GSDMD, Caspase-1, and IL-18 in the PFOS+NAC co-treatment group was significantly reduced compared to the PFOS group (Fig. 5F). In addition, the protein expression levels of NLRP3, GSDMD, GSDMD-N, Cleaved-Casp-1, IL-18, and IL-1β exhibited significant reductions in the PFOS+NAC co-treatment group compared to the PFOS group (Fig. 5G–M). Interestingly, the mRNA expression levels of pro-inflammatory cytokines (i.e., IFN-γ, IL-6, IL-8, and TNF-α) were significantly lower in the PFOS+NAC co-treatment group compared to the PFOS alone treatment group. In contrast, the mRNA levels of anti-inflammatory cytokines (i.e., IL-4 and IL-10) were significantly higher in the PFOS+NAC group compared to the PFOS group (Fig. 5N and O). These results indicate that oxidative stress may exert a substantial influence on the modulation of PFOS-induced pyroptosis.

3.6. *ROS inhibition alleviated PFOS exposure-induced lipid metabolism disorders in L8824 cells*

The impact of NAC pretreatment on PFOS-induced lipid metabolism in L8824 cells was examined next. As illustrated in Fig. 6A and B, NAC pre-treatment substantially improved lipid deposition induced by PFOS exposure in L8824 cells. In addition, NAC markedly decreased the expression levels of PPAR-γ and FASN in L8824 cells exposed to PFOS (Fig. 6C–E). Furthermore, according to Fig. 6F and G, NAC pre-treatment significantly reduced the PFOS-induced elevated mRNA expression level of genes involved in cellular lipid synthesis. Conversely, a significant increase in mRNA expression levels of genes related to cellular lipid catabolism was found. Therefore, the aforementioned findings indicate that suppression of excessive ROS generation can relieve the lipid metabolism disorder caused by PFOS exposure in L8824 cells.

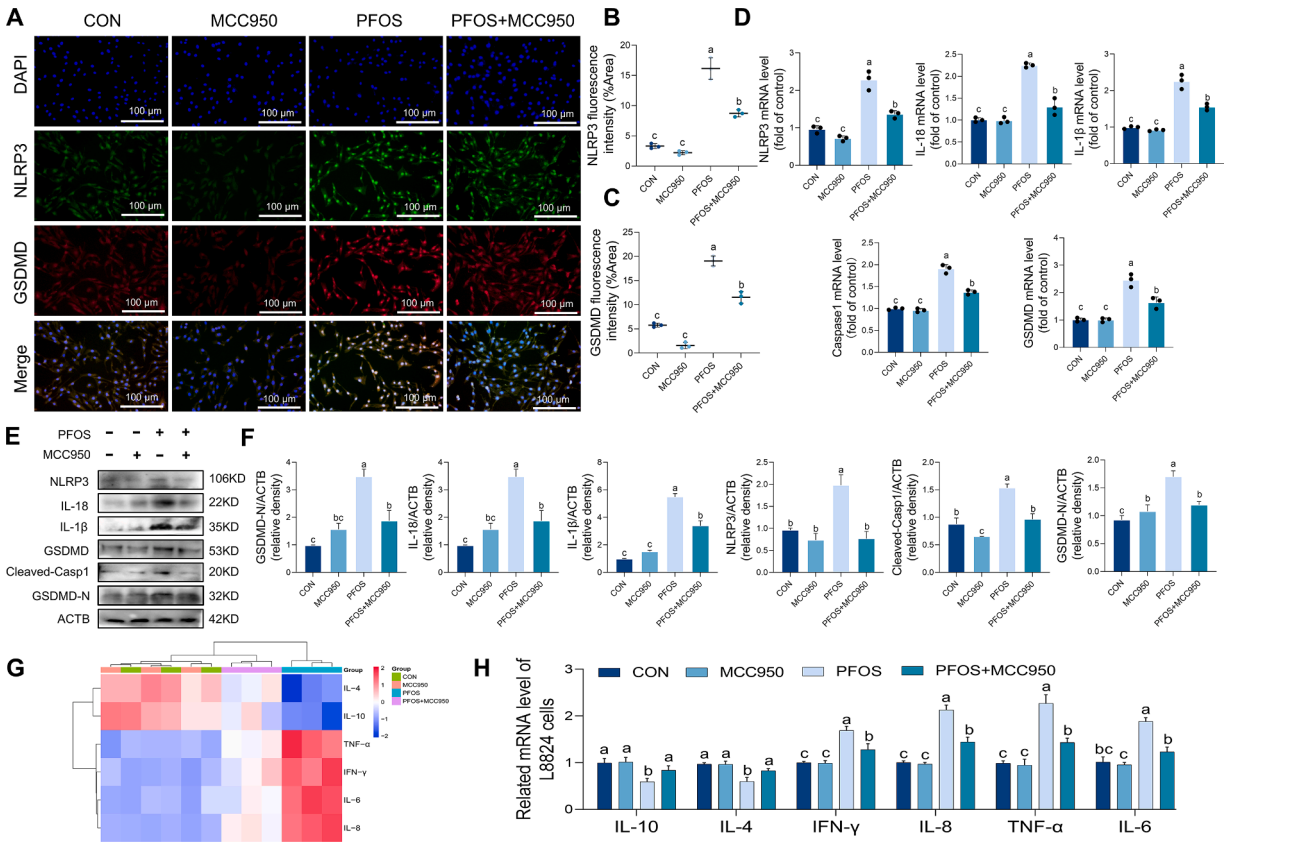

Fig. 7. Effects of MCC950 on PFOS-induced pyroptosis and inflammatory cytokine release in L8824 cells. (A–C) Immunofluorescence was employed to detect the fluorescence intensity of NLRP3 and GSDMD proteins in various treatment groups and to measure them. Scale bars: 100 μm. (D) The mRNA expression abundance of NLRP3, IL-1β, GSDMD, IL-18, and Caspase-1. (E, F) Results and quantitative analysis of pyroptosis genes (i.e., NLRP3, GSDMD, GSDMD-N, Cleaved-Casp-1, IL-1β, and IL-18) expression at the protein level. Heatmap (G) and quantitative bar graph (H) of mRNA expression abundance of inflammatory factors in each treatment group. The means ± SEM ($n = 3$) was used to present the experimental data. Significant differences among groups were denoted by variations in letters ($P < 0.05$). Conversely, groups with the same letters were considered not to have significant differences ($P \geq 0.05$).

3.7. NLRP3 inhibition alleviated PFOS exposure-induced pyroptosis and inflammatory cytokines release in L8824 cells

To verify the mechanism of action of NLRP3 in PFOS-induced pyroptosis in L8824 cells, L8824 cells were pre-treated with the NLRP3 inhibitor MCC950. As shown in representative images (Fig. 7A–C), the administration of MCC950 pre-treatment to PFOS exposure markedly reduced the fluorescence intensity from GSDMD (red) and NLRP3 (green). The mRNA expression levels of genes related to cellular pyroptosis (i.e., NLRP3, IL-18, IL-1β, Caspase-1, and GSDMD) were significantly reduced in the PFOS+MCC950 co-treatment group compared to the PFOS alone treatment group (Fig. 7D). Interestingly, the expression levels of the proteins GSDMD, GSDMD-N, IL-18, Cleaved-Casp-1, and IL-1β were significantly reduced in the PFOS+MCC950 co-treatment group compared to that of the PFOS-alone exposure group (Fig. 7E and F). As shown in Fig. 7G and H, pretreatment of L8824 cells with MCC950 significantly ameliorated the reduction in IL-4 and IL-10 mRNA expression abundance caused by PFOS exposure. Furthermore, NLRP3 inhibition significantly decreased the PFOS-induced increase in mRNA expression abundance of IL-8, IFN-γ, TNF-α, and IL-6. These results showed that PFOS-induced cellular injury was linked to pyroptosis mediated by NLRP3. The level of inflammatory cytokines can be effectively reduced through NLRP3 inhibition.

3.8. NLRP3 inhibition alleviated PFOS exposure-induced lipid metabolism disorders in L8824 cells

To evaluate the effect of the NLRP3 inflammasome on lipid metabolism in PFOS-treated L8824 cells, these cells were treated with MCC950 and a series of experiments was conducted. Compared with the PFOS group, the PFOS+MCC950 co-treatment group significantly inhibited PFOS-induced lipid deposition in L8824 cells (Fig. 8A and B). Moreover, according to Fig. 8C–E, the abundance of lipid synthesizing proteins (i.e., PPAR-γ and FASN) was significantly reduced in L8824 cells following MCC950 treatment. As illustrated in Fig. 8F and G, the mRNA expression levels of genes related to lipid synthesis were significantly reduced in the MCC950 and PFOS co-treatment groups compared to the PFOS group. Conversely, the mRNA expression level of genes related to lipid catabolism was significantly elevated. These results suggest that inhibition of NLRP3 can alleviate lipid metabolism disorders in L8824 cells exposed to PFOS.

3.9. Bioinformatics analysis of L8824 cells exposed to PFOS

The Pearson correlation coefficient was utilized to compare the correlation between cellular pyroptosis, inflammatory factors, and lipid metabolism (Fig. 9A). This correlation analysis demonstrated a significant negative relationship between the mRNA expression of NLRP3 and its downstream target genes in L8824 cells with lipolytic genes and anti-inflammatory factors. Additionally, a positive correlation was found between mRNA expression and lipid synthesis genes as well as pro-inflammatory factors. Metascape and STRING were used to further explore the relationship between genes following PFOS exposure. Visual network analysis of biological processes regulated by related proteins was conducted using Cytoscape. The connections among cellular pyroptosis, inflammatory factors, and lipid metabolism proteins have

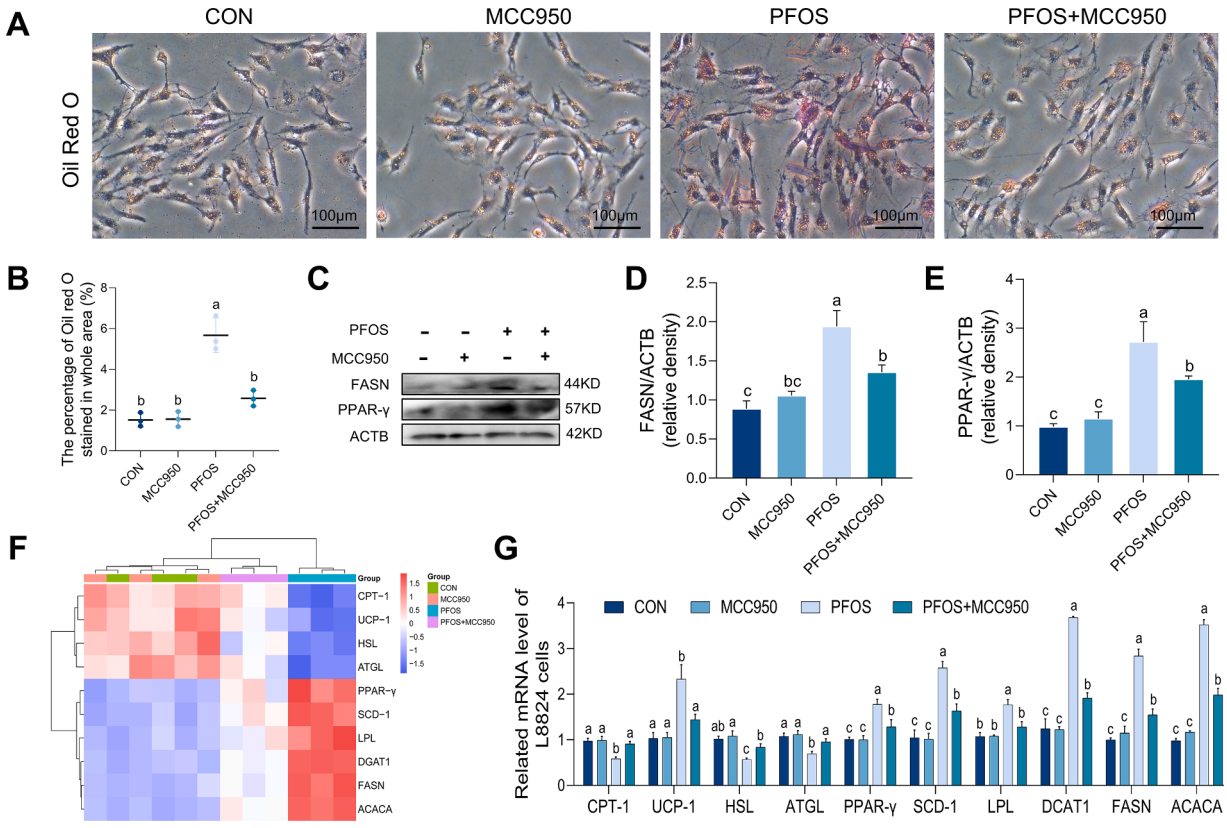

Fig. 8. Effects of MCC950 on PFOS-induced lipid metabolism disorder in L8824 cells. (A-B) Cells from various treatment groups were stained using Oil red O and analyzed quantitatively. Scale bars: 100 μm. (C–E) Results and quantitative analysis of lipid synthesis genes (PPAR-γ and FASN) expression at the protein level. Heatmap (F) and quantitative bar graph (G) of mRNA expression levels related to lipid synthesis (i.e., LPL, FASN, PPAR-γ, ACCα, DGAT1α, SCD-1) and lipid catabolic (i.e., UCP-1, ATGL, HSL, CPT-1) in L8824 cells under PFOS and MCC950 co-treatment. The means ± SEM ($n = 3$) was used to present the experimental data. Significant differences among groups were denoted by variations in letters ($P < 0.05$). Conversely, groups with the same letters were considered not to have significant differences ($P \geq 0.05$).

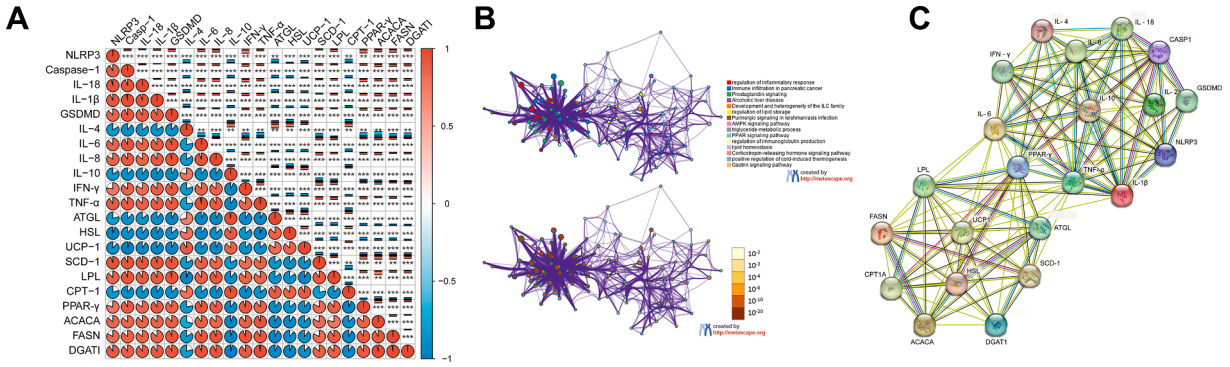

Fig. 9. Bioinformatics analysis of differentially expressed proteins in L8824 cells treatment with PFOS. (A) Correlation analysis of pyroptosis, inflammation, and lipid metabolism genes. (B) PPI network. (C) Diagram of the protein interaction network.

been depicted through STRING analysis, as demonstrated in Fig. 9B and C.

4. Discussion

Experimental evaluations of numerous studies on PFOS toxicity have identified PFOS as a pervasive organic pollutant with toxicity affecting multiple organs that adversely affects both ecosystem stability and public health. Currently, information on PFOS toxicity damage is generally concentrated on terrestrial organisms, while the potential mechanism of PFOS damage to aquatic organisms remains unclear. The liver is the main organ where environmental pollutants enter the body for metabolism and detoxification. PFOS exposure can cause hepatic steatosis, cancer, and bile acid metabolism disorders in mammals (Behr et al., 2020; Marques et al., 2020; Cao et al., 2022). In this experiment, the specific mechanisms underlying the cytotoxic damage to L8824 cells caused by PFOS exposure were examined through *in vitro* culture of grass carp hepatocytes. The findings indicate that PFOS has a dual effect on L8824 cells. Firstly, PFOS can induce pyroptosis by overproduction of ROS. Secondly, PFOS promotes the release of inflammatory factors that trigger inflammation and disrupt the lipid metabolism. NAC and MCC950 reduce pyroptosis and the subsequent inflammatory response in L8824 cells by reducing PFOS-induced excessive ROS production and inhibiting NLRP3 inflammasome activation, respectively; thereby, lipid

metabolism disorders are balanced and lipid deposition is reduced.

ROS play a crucial role in regulating cellular signaling pathways as a by-product of cellular metabolism. In mouse oocytes, exposure to PFOS results in oxidative stress through the buildup of ROS and reduced activity of antioxidant enzymes, which in turn affects the *in vitro* maturation of oocytes (Wei et al., 2021). The results of the present study demonstrate that exposure to PFOS led to a significant increase in ROS and MDA levels, which is indicative of oxidative stress. Additionally, a significant reduction in the activity of antioxidant enzymes was observed in response to PFOS treatment. This provides confirmation of the induction of oxidative stress in L8824 cells caused by PFOS exposure. ROS is assumed to be the primary molecule that triggers the activation of NLRP3 inflammasome when cells are stimulated by stressors (Kelley et al., 2019). Recent research indicated that NLRP3-mediated pyroptosis is a significant factor in liver injury induced by arsenic and polystyrene nanoplastics (Zhong et al., 2022). In addition, PFOS induces inflammatory responses in the lungs of mice by activating the NLRP3 inflammasome (Zhang et al., 2021). The findings of the present study demonstrate that PFOS administration prompted the activation of the NLRP3 inflammasome, subsequently enhancing the expression levels of both pyroptosis-related proteins and mRNAs. Notably, cellular pyroptosis is usually accompanied by the onset of an inflammatory response in the organism. Similar to previous findings, exposure to PFOS significantly augmented the mRNA expression levels of pro-inflammatory factors, and attenuated mRNA expression levels of anti-inflammatory factors correspondingly (Zhang et al., 2022b).

Numerous studies have shown that toxicants induce tissue damage by activating ROS-dependent NLRP3 inflammasome-mediated pyroptosis (Jiang et al., 2018; Wu et al., 2018; Qu et al., 2022). To further elucidate the involvement of the NLRP3 inflammasome in PFOS-induced hepatotoxicity, an additional experiment was conducted using MCC950, a pharmacological NLRP3 inhibitor. Remarkably, a pronounced reduction in the levels of pyroptosis-related proteins was observed upon NLRP3 inhibition, indicating the crucial role NLRP3 plays in the induction of pyroptosis following PFOS exposure. Moreover, the altered expression of inflammatory cytokines was restored following NLRP3 inhibition, thus confirming NLRP3-mediated pyroptosis as the mechanism underlying PFOS-induced hepatotoxicity. These experimental findings verify the necessity of NLRP3 for PFOS-triggered pyroptosis and indicate that pyroptosis mediated by NLRP3 is a plausible pathway leading to PFOS-induced liver damage. Further, altered expression levels of NLRP3 and downstream target genes after co-treatment of cells with NAC and PFOS identified ROS as upstream targets for NLRP3 inflammatory vesicle activation. These results show that ROS inhibition significantly attenuated PFOS-induced NLRP3 inflammasome activation and pyroptosis. Based on these findings, PFOS exposure caused L8824 cells pyroptosis and inflammatory factor release via ROS-mediated NLRP3 inflammasome activation.

PFOS disturbs lipid metabolism in both rodents and humans because its structure is similar to that of fatty acids (Lau et al., 2007; Fletcher et al., 2013). Evidence from clinical research suggests that NLRP3 inflammasome activation may influence metabolic disorders (Lee et al., 2013). Moreover, triglyceride levels were decreased in the livers of NLRP3-inflammasome-deficient mice compared with normal wild-type mice (Stienstra et al., 2011). Interestingly, a high expression abundance of IL-1β and NLRP3 has been detected in the liver of morbidly obese patients (Moschen et al., 2011). Zhao et al. (2017) demonstrated that fructose ingestion in mice stimulates the activation of the NLRP3 inflammasome in the liver and causes liver inflammation, which in turn leads to hepatic lipid metabolism disorder and the accumulation of lipids. Wang et al. (2014) demonstrated that PFOS can cause dysregulation of hepatic lipid metabolism in BALB/c mice. Mortensen et al. (2011) found higher PFOS values in the liver of fish fed a PFOS diet. In the present study, PFOS treatment significantly affected the expression of lipid metabolism-related genes and induced lipid metabolism disorders in L8824 cells. Correspondingly, NAC and MCC950 inhibitor intervention improved lipid metabolism disorders and alleviated PFOS-induced lipid deposition in L8824 cells. PFOS exposure induces pyroptosis and the release of inflammatory factors by causing oxidative stress; this overproduction of inflammatory factors interferes with the expression levels of genes related to lipid metabolism, thus inducing lipid metabolism disorders and causing lipid deposition. Therefore, these results show that PFOS exposure caused L8824 cell lipid metabolism disorders via ROS-mediated NLRP3 inflammasome activation.

The induction of lipid metabolism disorders in hepatocytes by PFOS can be attributed to the excessive accumulation of ROS, which subsequently triggers hepatocyte pyroptosis and amplifies hepatocyte inflammation. Inhibition of this NLRP3 inflammasome activation alleviated L8824 cell pyroptosis and lipid metabolism disorders induced by PFOS. Further, inhibition of excessive ROS production effectively mitigated the activation of the NLRP3 inflammasome, which in turn prevented pyroptosis of L8824 cells and ameliorated disturbances in the lipid metabolism. Hence, PFOS exposure caused L8824 cell pyroptosis and lipid metabolism disorders via ROS-mediated NLRP3 inflammasome activation. The results of this study are of great value to better understand the hepatotoxicity of PFOS and can be used as a reference for toxicological studies on PFOS in aquatic organisms.

CRediT authorship contribution statement

Bendong Shi: Writing – original draft, Investigation. **Zhuoqi Zhang:** Methodology, Supervision. **Jiao Xing:** Data curation, Methodology. **Qiaohan Liu:** Investigation, Software. **Jingzeng Cai:** Conceptualization, Supervision. **Ziwei Zhang:** Funding acquisition, Methodology, Conceptualization, Writing – review & editing.

Declaration of competing interest

The authors declare that they have no known competing financial interests or personal relationships that could have appeared to influence the work reported in this paper.

Data availability

Data will be made available on request.

Acknowledgment

This study was supported by Excellent Youth Foundation of Heilongjiang Province of China. (YQ2021C021)

Supplementary materials

Supplementary material associated with this article can be found, in the online version, at doi:10.1016/j.aquatox.2024.106839.

References

Barbosa Machado Torres, F., Guida, Y., Weber, R., Machado Torres, J.P., 2022. Brazilian overview of per- and polyfluoroalkyl substances listed as persistent organic pollutants in the stockholm convention. Chemosphere 291, 132674.

Behr, A.C., Kwiatkowski, A., Stahlman, M., Schmidt, F.F., Luckert, C., Braeuning, A., Buhrke, T., 2020. Impairment of bile acid metabolism by perfluorooctanoic acid (PFOA) and perfluorooctanesulfonic acid (PFOS) in human HepaRG hepatoma cells. Arch. Toxicol. 94, 1673–1686.

Buck, R.C., Franklin, J., Berger, U., Conder, J.M., Cousins, I.T., de Voogt, P., Jensen, A.A., Kannan, K., Mabury, S.A., van Leeuwen, S.P., 2011. Perfluoroalkyl and polyfluoroalkyl substances in the environment: terminology, classification, and origins. Integr. Environ. Assess. Manag. 7, 513–541.

Cai, J., Guan, H., Jiao, X., Yang, J., Chen, X., Zhang, H., Zheng, Y., Zhu, Y., Liu, Q., Zhang, Z., 2021. NLRP3 inflammasome mediated pyroptosis is involved in cadmium exposure-induced neuroinflammation through the IL-1beta/IkB-alpha-NF-kappaB-NLRP3 feedback loop in swine. Toxicology 453, 152720.

Cai, J., Guan, H., Li, D., Shi, B., Jiang, Y., Qiao, S., Liu, Q., Fang, C., Zhang, Z., 2023a. New insights into microalgal astaxanthin's effect on Lambda-cyhalothrin-induced

lymphocytes immunotoxicity in Cyprinus carpio: involving miRNA-194-5p-FoxO1-mediated-mitophagy and pyroptosis. Fish Shellfish Immunol. 141, 109046.
Cai, J., Liu, P., Zhang, X., Shi, B., Jiang, Y., Qiao, S., Liu, Q., Fang, C., Zhang, Z., 2023b. Micro-algal astaxanthin improves lambda-cyhalothrin-induced necroptosis and inflammatory responses via the ROS-mediated NF-kappaB signaling in lymphocytes of carp (Cyprinus carpio L.). Fish Shellfish Immunol. 139, 108929.
Cao, L., Guo, Y., Chen, Y., Hong, J., Wu, J., Hangbiao, J., 2022. Per-/polyfluoroalkyl substance concentrations in human serum and their associations with liver cancer. Chemosphere 296, 134083.
Chen, T., Zhang, L., Yue, J.Q., Lv, Z.Q., Xia, W., Wan, Y.J., Li, Y.Y., Xu, S.Q., 2012. Prenatal PFOS exposure induces oxidative stress and apoptosis in the lung of rat offspring. Reprod. Toxicol. 33, 538–545.
Chen, Y., Jiang, L., Zhang, R., Shi, Z., Xie, C., Hong, Y., Wang, J., Cai, Z., 2022. Spatially revealed perfluorooctane sulfonate-induced nephrotoxicity in mouse kidney using atmospheric pressure MALDI mass spectrometry imaging. Sci. Total Environ. 838, 156380.
Chi, Q., Xu, T., He, Y., Li, Z., Tang, X., Fan, X., Li, S., 2022. Polystyrene nanoparticle exposure supports ROS-NLRP3 axis-dependent DNA-NET to promote liver inflammation. J. Hazard. Mater. 439, 129502.
Chu, K., Lu, Y., Hua, Z., Liu, Y., Ma, Y., Gu, L., Gao, C., Yu, L., Wang, Y., 2022. Perfluoroalkyl acids (PFAAs) in the aquatic food web of a temperate urban lake in East China: bioaccumulation, biomagnification, and probabilistic human health risk. Environ. Pollut. 296, 118748.
Cui, J., Wang, P., Yan, S., Liang, Y., Liu, D., Ren, S., 2022. Perfluorooctane sulfonate induces dysfunction of human umbilical vein endothelial cells via ferroptosis pathway. Toxics 10, 503.
Dong, B., Jiang, Y., Shi, B., Zhang, Z., Zhang, Z., 2023. Selenomethionine alleviates decabromodiphenyl ether-induced oxidative stress and ferroptosis via the NRF2/GPX4 pathway in the chicken brain. J. Hazard. Mater. 465, 133307.
Fletcher, T., Galloway, T.S., Melzer, D., Holcroft, P., Cipelli, R., Pilling, L.C., Mondal, D., Luster, M., Harries, L.W., 2013. Associations between PFOA, PFOS and changes in the expression of genes involved in cholesterol metabolism in humans. Environ. Int. 57-58, 2–10.
Foord, C.S., Szabo, D., Robb, K., Clarke, B.O., Nugegoda, D., 2024. Hepatic concentrations of per- and polyfluoroalkyl substances (PFAS) in dolphins from south-east Australia: highest reported globally. Sci. Total Environ. 908, 168438.
Gao, Y., Ma, Y., Xie, D., Jiang, H., 2022. ManNAc protects against podocyte pyroptosis via inhibiting mitochondrial damage and ROS/NLRP3 signaling pathway in diabetic kidney injury model. Int. Immunopharmacol. 107, 108711.
Guida, Y., Torres, F.B.M., Barizon, R.R.M., Assalin, M.R., Rosa, M.A., 2023. Confirming sulfluramid (EtFOSA) application as a precursor of perfluorooctanesulfonic acid (PFOS) in Brazilian agricultural soils. Chemosphere 325, 138370.
Harrad, S., Wemken, N., Drage, D.S., Abdallah, M.A., Coggins, A.M., 2019. Perfluoroalkyl substances in drinking water, indoor air and dust from ireland: implications for human exposure. Environ. Sci. Technol. 53, 13449–13457.
Hu, Q., Wei, B., Wei, L., Hua, K., Yu, X., Li, H., Ji, H., 2015. Sodium tanshinone IIA sulfonate ameliorates ischemia-induced myocardial inflammation and lipid accumulation in Beagle dogs through NLRP3 inflammasome. Int. J. Cardiol. 196, 183–192.
Jiang, C., Jiang, L., Li, Q., Liu, X., Zhang, T., Dong, L., Liu, T., Liu, L., Hu, G., Sun, X., Jiang, L., 2018. Acrolein induces NLRP3 inflammasome-mediated pyroptosis and suppresses migration via ROS-dependent autophagy in vascular endothelial cells. Toxicology 410, 26–40.
Jiang, L., Hong, Y., Xiao, P., Wang, X., Zhang, J., Liu, E., Li, H., Cai, Z., 2022. The role of fecal microbiota in liver toxicity induced by perfluorooctane sulfonate in male and female mice. Environ. Health Perspect. 130, 67009.
Kelley, N., Jeltema, D., Duan, Y., He, Y., 2019. The NLRP3 inflammasome: an overview of mechanisms of activation and regulation. Int. J. Mol. Sci. 20, 3328.
Lau, C., Anitole, K., Hodes, C., Lai, D., Pfahles-Hutchens, A., Seed, J., 2007. Perfluoroalkyl acids: a review of monitoring and toxicological findings. Toxicol. Sci. 99, 366–394.
Lee, H., Sung, E.J., Seo, S., Min, E.K., Lee, J.Y., Shim, I., Kim, P., Kim, T.Y., Lee, S., Kim, K.T., 2021. Integrated multi-omics analysis reveals the underlying molecular mechanism for developmental neurotoxicity of perfluorooctanesulfonic acid in zebrafish. Environ. Int. 157, 106802.
Lee, H.M., Kim, J.J., Kim, H.J., Shong, M., Ku, B.J., Jo, E.K., 2013. Upregulated NLRP3 inflammasome activation in patients with type 2 diabetes. Diabetes 62, 194–204.
Li, D., Zhang, K., Xu, C., Jiang, Y., Shan, J., Zhang, Z., Cai, J., 2023a. Cypermethrin induces apoptosis, autophagy and inflammation via ERS-ROS-NF-kappaB axis in hepatocytes of carp (Cyprinus carpio). Pestic. Biochem. Physiol. 196, 105625.
Li, X., Bai, Y., Bi, Y., Wu, Q., Xu, S., 2023b. Baicalin suppressed necroptosis and inflammation against chlorpyrifos toxicity; involving in ER stress and oxidative stress in carp gills. Fish Shellfish Immunol. 139, 108883.
Liang, L., Pan, Y., Bin, L., Liu, Y., Huang, W., Li, R., Lai, K.P., 2022. Immunotoxicity mechanisms of perfluorinated compounds PFOA and PFOS. Chemosphere 291, 132892.
Liu, J., Yang, G., Zhang, H., 2023. Glyphosate-triggered hepatocyte ferroptosis via suppressing Nrf2/GSH/GPX4 axis exacerbates hepatotoxicity. Sci. Total Environ. 862, 160839.
Liu, Q., Du, P., Zhu, Y., Zhang, X., Cai, J., Zhang, Z., 2022a. Thioredoxin reductase 3 suppression promotes colitis and carcinogenesis via activating pyroptosis and necrosis. Cell Mol. Life Sci. 79, 106.
Liu, Z., Zhou, J., Xu, Y., Lu, J., Chen, J., Wang, J., 2022b. Distributions and sources of traditional and emerging per- and polyfluoroalkyl substances among multiple environmental media in the Qiantang River watershed, China. RSC Adv. 12, 21247–21254.
Lo, C.W., Yen, C.C., Chen, C.Y., Chen, H.W., Lii, C.K., 2023. Benzyl isothiocyanate attenuates activation of the NLRP3 inflammasome in Kupffer cells and improves diet-induced steatohepatitis. Toxicol. Appl. Pharmacol. 462, 116424.
Luo, D., Chen, S., Wang, X., Wang, Y., Khoso, P.A., Xu, S., Li, S., 2023. Unraveling the mechanism of quercetin alleviating perfluorooctane sulfonate-induced apoptosis in grass carp (Ctenopharyngodon idellus) hepatocytes: AMPK/mTOR-mediated mitophagy. Aquat. Toxicol. 265, 106769.
Ma, X., Ma, J., Leng, T., Yuan, Z., Hu, T., Liu, Q., Shen, T., 2023. Advances in oxidative stress in pathogenesis of diabetic kidney disease and efficacy of TCM intervention. Ren. Fail. 45, 2146512.
Mahapatra, A., Gupta, P., Suman, A., Ray, S.S., Malafaia, G., Singh, R.K., 2023. Unraveling the mechanisms of perfluorooctanesulfonic acid-induced dopaminergic neurotoxicity and microglial activation in developing zebrafish. Sci. Total. Environ. 887, 164030.
Mao, W., Li, M., Xue, X., Cao, W., Wang, X., Xu, F., Jiang, W., 2023. Bioaccumulation and toxicity of perfluorooctanoic acid and perfluorooctane sulfonate in marine algae Chlorella sp. Sci. Total. Environ. 870, 161882.
Marques, E., Pfohl, M., Auclair, A., Jamwal, R., Barlock, B.J., Sammoura, F.M., Goedken, M., Akhlaghi, F., Slitt, A.L., 2020. Perfluorooctanesulfonic acid (PFOS) administration shifts the hepatic proteome and augments dietary outcomes related to hepatic steatosis in mice. Toxicol. Appl. Pharmacol. 408, 115250.
Mortensen, A.S., Letcher, R.J., Cangialosi, M.V., Chu, S., Arukwe, A., 2011. Tissue bioaccumulation patterns, xenobiotic biotransformation and steroid hormone levels in Atlantic salmon (Salmo salar) fed a diet containing perfluoroactane sulfonic or perfluorooctane carboxylic acids. Chemosphere 83, 1035–1044.
Moschen, A.R., Molnar, C., Enrich, B., Geiger, S., Ebenbichler, C.F., Tilg, H., 2011. Adipose and liver expression of interleukin (IL)-1 family members in morbid obesity and effects of weight loss. Mol. Med. 17, 840–845.
Qu, J., Zhang, S., He, W., Liu, S., Mao, X., Yin, L., Yue, D., Zhang, P., Huang, K., Chen, X., 2022. Crucial function of caveolin-1 in deoxynivalenol-induced enterotoxicity by activating ROS-dependent NLRP3 inflammasome-mediated pyroptosis. J. Agric. Food Chem. 70, 12968–12981.
Shang, S., Sun, F., Zhu, Y., Yu, J., Yu, L., Shao, W., Wang, Z., Yi, X., 2023. Sevoflurane preconditioning improves neuroinflammation in cerebral ischemia/reperfusion induced rats through ROS-NLRP3 pathway. Neurosci. Lett. 801, 137164.
Shi, X., Xu, T., Li, X., Sun, X., Zhang, W., Liu, X., Wang, Y., Zhang, Y., Xu, S., 2023. ROS mediated pyroptosis-M1 polarization crosstalk participates in inflammation of chicken liver induced by bisphenol A and selenium deficiency. Environ. Pollut. 324, 121392.
Stienstra, R., van Diepen, J.A., Tack, C.J., Zaki, M.H., van de Veerdonk, F.L., Perera, D., Neale, G.A., Hooiveld, G.J., Hijmans, A., Vroegrijk, I., van den Berg, S., Romijn, J., Rensen, P.C., Joosten, L.A., Netea, M.G., Kanneganti, T.D., 2011. Inflammasome is a central player in the induction of obesity and insulin resistance. Proc. Natl. Acad. Sci. U. S. A. 108, 15324–15329.
Tilg, H., Adolph, T.E., Dudek, M., Knolle, P., 2021. Non-alcoholic fatty liver disease: the interplay between metabolism, microbes and immunity. Nat. Metab. 3, 1596–1607.
Wang, D., Tan, Z., Yang, J., Li, L., Li, H., Zhang, H., Liu, H., Liu, Y., Wang, L., Li, Q., Guo, H., 2023a. Perfluorooctane sulfonate promotes atherosclerosis by modulating M1 polarization of macrophages through the NF-kappaB pathway. Ecotoxicol. Environ. Saf. 249, 114384.
Wang, L., Wang, Y., Liang, Y., Li, J., Liu, Y., Zhang, J., Zhang, A., Fu, J., Jiang, G., 2014. PFOS induced lipid metabolism disturbances in BALB/c mice through inhibition of low density lipoproteins excretion. Sci. Rep. 4, 4582.
Wang, L.Q., Liu, T., Yang, S., Sun, L., Zhao, Z.Y., Li, L.Y., She, Y.C., Zheng, Y.Y., Ye, X.Y., Bao, Q., Dong, G.H., Li, C.W., Cui, J., 2021. Perfluoroalkyl substance pollutants activate the innate immune system through the AIM2 inflammasome. Nat. Commun. 12, 2915.
Wang, P., Liu, D., Yan, S., Cui, J., Liang, Y., Ren, S., 2022. Adverse effects of perfluorooctane sulfonate on the liver and relevant mechanisms. Toxics 10, 265.
Wang, Q., Yao, X., Jiang, N., Zhang, J., Liu, G., Li, X., Wang, C., Yang, Z., Wang, J., Zhu, L., Wang, J., 2023b. Environmentally relevant concentrations of butyl benzyl phthalate triggered oxidative stress and apoptosis in adult zebrafish (Danio rerio) liver: combined analysis at physiological and molecular levels. Sci. Total Environ. 858, 160109.
Wang, T., Xu, H., Guo, Y., Li, Z., Ye, H., Wu, L., Guo, Y., Wang, D., 2023c. Perfluorodecanoic acid promotes adipogenesis via NLRP3 inflammasome-mediated pathway in HepG2 and 3T3-L1 cells. Food Chem. Toxicol. 171, 113520.
Wang, X., Zhang, H., He, X., Liu, J., Yao, Z., Zhao, H., Yu, D., Liu, B., Liu, T., Zhao, W., 2023d. Contamination of per-and polyfluoroalkyl substances in the water source from a typical agricultural area in North China. Front. Environ. Sci. 10, 2545.
Wei, K.N., Wang, X.J., Zeng, Z.C., Gu, R.T., Deng, S.Z., Jiang, J., Xu, C.L., Li, W., Wang, H.L., 2021. Perfluorooctane sulfonate affects mouse oocyte maturation *in vitro* by promoting oxidative stress and apoptosis induced bymitochondrial dysfunction. Ecotoxicol. Environ. Saf. 225, 112807.
Wong, F., Shoeib, M., Katsoyiannis, A., Eckhardt, S., Stohl, A., Bohlin-Nizzetto, P., Li, H., Fellin, P., Su, Y., Hung, H., 2018. Assessing temporal trends and source regions of per- and polyfluoroalkyl substances (PFASs) in air under the Arctic Monitoring and Assessment Programme (AMAP). Atmos. Environ. 172, 65–73.
Wu, M., Yang, Z., Zhang, C., Shi, Y., Han, W., Song, S., Mu, L., Du, C., Shi, Y., 2021. Inhibition of NLRP3 inflammasome ameliorates podocyte damage by suppressing lipid accumulation in diabetic nephropathy. Metabolism 118, 154748.
Wu, X., Zhang, H., Qi, W., Zhang, Y., Li, J., Li, Z., Lin, Y., Bai, X., Liu, X., Chen, X., Yang, H., Xu, C., Zhang, Y., Yang, B., 2018. Nicotine promotes atherosclerosis via ROS-NLRP3-mediated endothelial cell pyroptosis. Cell Death Dis. 9, 171.
Xin, S., Li, W., Zhang, X., He, Y., Chu, J., Zhou, X., Zhang, Y., Liu, X., Wang, S., 2023. Spatiotemporal variations and bioaccumulation of per- and polyfluoroalkyl

substances and oxidative conversion of precursors in shallow lake water. Chemosphere 313, 137527.
Yang, B., Chen, Y., Shi, J., 2019. Reactive oxygen species (ROS)-based nanomedicine. Chem. Rev. 119, 4881–4985.
Yang, X., Liu, P., Cui, Y., Song, M., Zhang, X., Zhang, C., Jiang, Y., Li, Y., 2022. T-2 toxin caused mice testicular inflammation injury via ROS-mediated NLRP3 inflammasome activation. J. Agric. Food Chem. 70, 14043–14051.
Yao, X.F., Cao, J., Xu, L.M., Sun, X.C., Kang, J., Yang, G., Jiang, L.P., Geng, C.Y., Gao, C. Z., Zhong, L.F., Ma, Y.F., 2014. Perfluorooctane sulfonate blocked autophagy flux and induced lysosome membrane permeabilization in HepG2 cells. Food Chem. Toxicol. 67, 96–104.
Yao, Y., Chen, T., Wu, H., Yang, N., Xu, S., 2023a. Melatonin attenuates bisphenol A-induced colon injury by dual targeting mitochondrial dynamics and Nrf2 antioxidant system via activation of SIRT1/PGC-1alpha signaling pathway. Free Radic. Biol. Med. 195, 13–22.
Yao, Y., Zhu, W., Han, D., Shi, X., Xu, S., 2023b. New insights into how melatonin ameliorates bisphenol A-induced colon damage: inhibition of NADPH oxidase. J. Agric. Food Chem. 71, 2566–2578.
Zareitalabad, P., Siemens, J., Hamer, M., Amelung, W., 2013. Perfluorooctanoic acid (PFOA) and perfluorooctanesulfonic acid (PFOS) in surface waters, sediments, soils and wastewater - A review on concentrations and distribution coefficients. Chemosphere 91, 725–732.
Zhang, H., Lu, H., Yu, L., Yuan, J., Qin, S., Li, C., Ge, R.S., Chen, H., Ye, L., 2021. Effects of gestational exposure to perfluorooctane sulfonate on the lung development of offspring rats. Environ. Pollut. 272, 115535.
Zhang, Y., Wu, X., Zhu, K., Liu, S., Yang, Y., Yuan, D., Wang, T., He, Y., Dun, Y., Wu, J., Zhang, C., Zhao, H., 2022a. Icariin attenuates perfluorooctane sulfonate-induced testicular toxicity by alleviating Sertoli cell injury and downregulating the p38MAPK/MMP9 pathway. Food Funct. 13, 3674–3689.
Zhang, Y., Yin, K., Wang, D., Wang, Y., Lu, H., Zhao, H., Xing, M., 2022b. Polystyrene microplastics-induced cardiotoxicity in chickens via the ROS-driven NF-kappaB-NLRP3-GSDMD and AMPK-PGC-1alpha axes. Sci. Total. Environ. 840, 156727.
Zhao, X.J., Yang, Y.Z., Zheng, Y.J., Wang, S.C., Gu, H.M., Pan, Y., Wang, S.J., Xu, H.J., Kong, L.D., 2017. Magnesium isoglycyrrhizinate blocks fructose-induced hepatic NF-kappaB/NLRP3 inflammasome activation and lipid metabolism disorder. Eur. J. Pharmacol. 809, 141–150.
Zhao, X.J., Yang, Y.Z., Zheng, Y.J., Wang, S.C., Gu, H.M., Pan, Y., Wang, S.J., Xu, H.J., Kong, L.D., 2021. Corrigendum to "Magnesium isoglycyrrhizinate blocks fructose-induced hepatic NF-kappaB/NLRP3 inflammasome activation and lipid metabolism disorder. Eur. J. Pharmacol. 15 (2017), 809, 141-150. Eur J Pharmacol 909, 174440.
Zhong, G., Rao, G., Tang, L., Wu, S., Tang, Z., Huang, R., Ruan, Z., Hu, L., 2022. Combined effect of arsenic and polystyrene-nanoplastics at environmentally relevant concentrations in mice liver: activation of apoptosis, pyroptosis and excessive autophagy. Chemosphere 300, 134566.